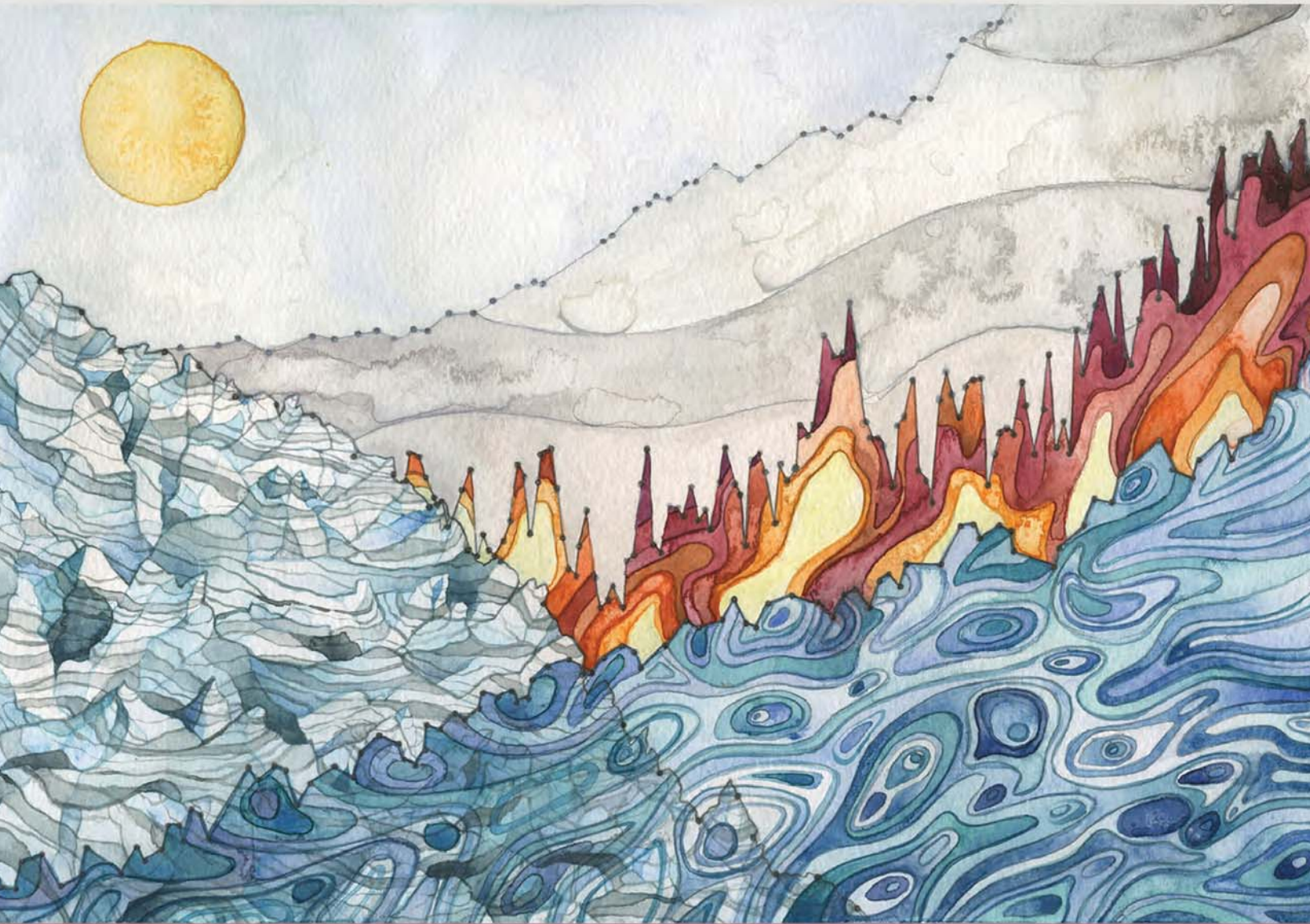


STATE OF THE CLIMATE IN 2015



Special Supplement to the
Bulletin of the American Meteorological Society
Vol. 97, No. 8, August 2016

westward spreading and weakening of the prominent fresh anomaly generated west of Australia circa 2011.

Seasonal variations of SSS anomalies in 2015 (Fig. 3.8) from BASS (Xie et al. 2014) show the buildup of anomalously fresh water associated with the tropical Pacific and western tropical Atlantic ITCZs (including just offshore of the Orinoco and Amazon Rivers), the increase in SSS in the tropical warm pool, and the decrease in fresh anomalies under the South Pacific convergence zone (SPCZ). Despite the lower accuracies of the satellite data relative to that of the Argo data, their higher spatial and temporal sampling allows higher spatial and temporal resolution maps than are possible using in situ data alone.

Sea surface salinity trends for 2005–15 exhibit striking patterns in all three oceans (Fig. 3.7c). These trends are estimated by local linear fits to annual average SSS maps from Argo data with a starting year of 2005, because that is when Argo coverage became near-global. Near the salinity maxima in each basin (mostly in the subtropics but closer to 30°S in the Indian Ocean), there are regions of increasing salinity, especially in the North Pacific to the west of Hawaii. In contrast, there are regions in the Southern Ocean where the trend is toward freshening. Again, these patterns are reminiscent of the multidecadal changes discussed above and suggest an intensification of the hydrological cycle over the ocean, even over the last 11 years. There is a strong freshening trend in much of the subpolar North Atlantic, roughly coincident with anomalously low upper ocean heat content there (see Fig. 3.4) suggesting an eastward expansion of the subpolar gyre that may be linked to reductions in the AMOC over the past decade (section 3h). In addition to these patterns there is a freshening trend in the eastern Indian Ocean, probably owing to a lingering signature of the strong 2010–12 La Niña, as discussed above. Freshening trends are also apparent in the eastern tropical Pacific and the South China Sea. The region to the northwest of the Gulf Stream is trending saltier, as well as warmer (section 3c).

3) SUBSURFACE SALINITY—J. Reagan, T. Boyer, C. Schmid, and R. Locarnini

Atlantic Ocean basin-average monthly salinity anomalies for 0–1500 m depth displayed a pattern

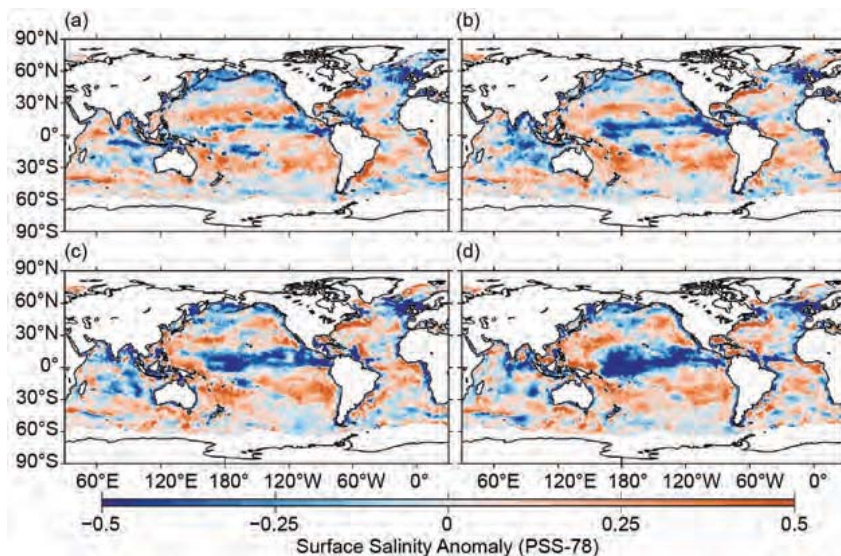


FIG. 3.8. Seasonal maps of SSS anomalies (colors) from monthly blended maps of satellite and in situ salinity data (BASS; Xie et al. 2014) relative to monthly climatological salinity fields from WOA 2009 for (a) Dec–Feb 2014/15, (b) Mar–May 2015, (c) Jun–Aug 2015, and (d) Sep–Nov 2015. Areas with maximum monthly errors exceeding 10 PSS-78 are left white.

during 2015 similar to the previous 10 years, with salty anomalies above 700 m and fresh anomalies below (Fig. 3.9a). From 2014 to 2015 salinity increased in the upper 300 m of the Atlantic, reaching a maximum increase of ~ 0.01 near the surface (Fig. 3.9b). The Pacific Ocean has exhibited fresh anomalies of about -0.02 from 200 to 500 m over the last five years (Fig. 3.9c). However, the upper 75 m was about -0.04 fresher in 2015, in contrast to salty conditions there from mid-2008 to mid-2014. This change reflects the enhanced precipitation along the ITCZ (see Fig. 3.12d) and anomalous eastward equatorial currents (see Fig. 3.19) during the 2015 El Niño (see section 4b). Salty anomalies from 100 to 200 m have been present since 2011. From 2014 to 2015 the Pacific (Fig. 3.9d) freshened in the upper 75 m, approaching about -0.03 at 30 m, and became saltier from 100 to 200 m, approaching ~ 0.01 at 125 m. The Indian Ocean continued to show similar salinity anomaly structure to that of the previous two years, with a fresh surface anomaly from 0 to 75 m, salty subsurface anomaly from 100 to 300 m, a slightly fresh anomaly (maximum of about -0.01) from 400 to 600 m, and a slightly salty anomaly (maximum of ~ 0.01) from 600 to 800 m (Fig. 3.9e). From 2014 to 2015 there was weak freshening (maximum of about -0.01 at 50 m) near the surface and salinification from 100 to 200 m, with a maximum of ~ 0.014 at 150 m (Fig. 3.9f).

North Atlantic 2015 volume-weighted salinity anomalies from 0 to 1500 m (Fig. 3.10a) were mostly positive, with values >0.10 along the Gulf Stream. The eastern portion of the subpolar gyre in the North

Atlantic exhibited a large (about -0.10) fresh anomaly. This fresh feature coincided with anomalously cool upper ocean heat content (see Fig. 3.4). The South Atlantic was dominated by positive salinity anomalies in 2015, with fresh anomalies south of 40°S , perhaps reflecting an anomalously northward position of the low salinity subantarctic front. From 2014 to 2015, positive salinity anomalies in the subtropics persisted with little change in strength, while the freshening north of the Azores Islands continued to strengthen (Fig. 3.10b).

The Indian Ocean displayed a dipole of salinity anomalies north of the equator during 2015, with salty anomalies in the Arabian Sea and fresh anomalies in the Bay of Bengal (Fig. 3.10a). Salty anomalies along the equator transitioned to fresh anomalies across the entire basin south of 15°S to 30°S . These fresh anomalies strengthened east of Madagascar from 2014 to 2015 but weakened west of Australia (Fig. 3.10b) as discussed in section 3d2. From 35°S to 50°S there was a transition from salty to fresh salinity anomalies, likely due to the position of the subantarctic front in 2015 (Fig. 3.10a).

The North Pacific, north of 20°N , was dominated by fresh anomalies in 2015; however, in the northeast

Pacific there was a salty anomaly (Fig. 3.10a) in close proximity to a region of anomalously warm SSTs (see Fig. 3.1). The warm SSTs were at least partly due to a persistent atmospheric ridge in the region (Bond et al. 2015). With ridging, less precipitation and more evaporation are expected. This expectation was partially met (see Fig. 3.12) and likely to have been partially responsible for the observed salty anomaly strengthening from 2014 to 2015 (Fig. 3.10b). The subtropical North Pacific was anomalously salty in 2015, consistent with the 2015 $P-E$ anomalies (see Fig. 3.12). Salty anomalies were present in the subtropical South Pacific in 2015, with fresh anomalies along the SPCZ. These tropical and subtropical salinity anomaly features were mostly enhanced when compared to 2014, with the exception of a weakening

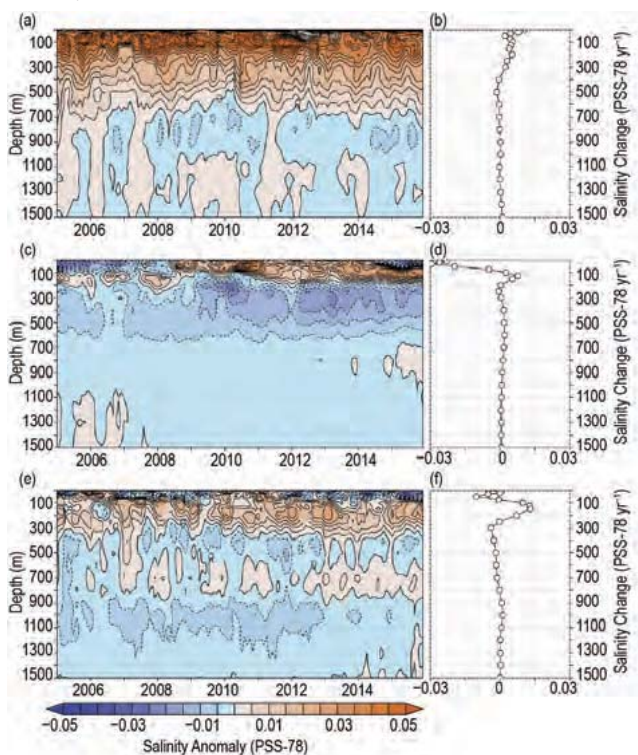


FIG. 3.9. Average monthly salinity anomalies from 0–1500 m for the (a) Atlantic from 2005–15 and (b) the change from 2014 to 2015; (c) Pacific from 2005–15 and (d) the change from 2014 to 2015; and (e) Indian from 2005–15 and (f) the change from 2014 to 2015. Data were smoothed using a 3-month running mean. Anomalies are relative to the long-term WOA 2009 monthly salinity climatology (Antonov et al. 2010).

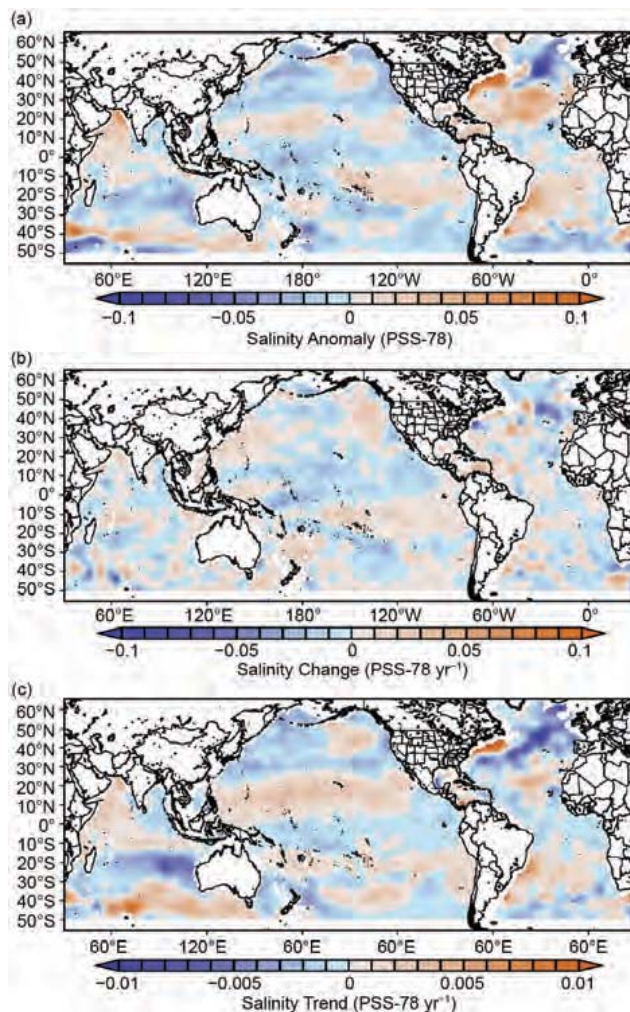


FIG. 3.10. Near-global 0–1500 m volume-weighted salinity anomalies (a) for 2015, (b) change from 2014 to 2015, and (c) linear trend from 2005 to 2015 (yr^{-1}). Anomalies are relative to the long-term WOA 2009 monthly salinity climatology (Antonov et al. 2010). Annual figures were computed by averaging the 12 monthly salinity anomalies over calendar years.

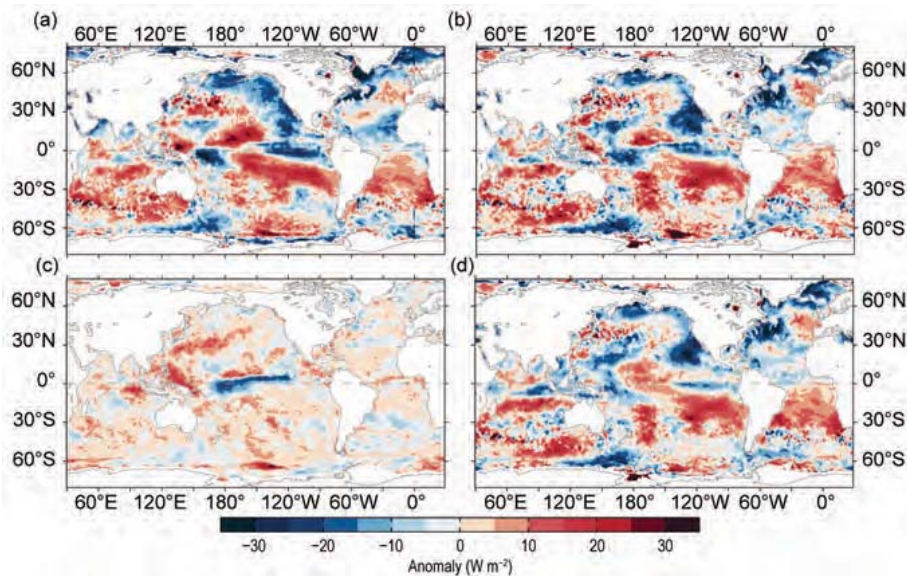


FIG. 3.11. (a) Surface heat flux (Q_{net}) anomalies for 2015 relative to a 5-year (2010–14) mean. Positive values denote ocean heat gain. Panels (b), (c), and (d) are the 2015–2014 anomaly tendencies for Q_{net} , surface radiation (SW+LW), and turbulent heat fluxes (LH+SH), respectively. Positive anomalies denote that the ocean gained more heat in 2015 than in 2014. LH+SH are produced by the OAFIux high-resolution satellite-based analysis, and SW+LW by the NASA FLASHflux project.

positive salinity anomaly over the central subtropical North Pacific in 2015 (Fig. 3.10b). The South Pacific enhancement from 2014 to 2015 is inconsistent with 2015 $P-E$ anomalies (see Fig. 3.12).

The 2005–15 linear trends of the 0–1500 m salinity anomalies (Fig. 3.10c) reveal strong similarities to SSS trends over the same time period (see Fig. 3.7c and discussion above). This match is not surprising as most of the salinity variability from 0 to 1500 m over the global ocean occurs in the upper 300 m (Fig. 3.9). The large ($> -0.01 \text{ yr}^{-1}$) freshening trend in the North Atlantic subpolar gyre could be partially responsible for the observed decline in the strength of the AMOC (Smeed et al. 2014).

e. *Ocean surface heat, freshwater, and momentum fluxes*—
L. Yu, R. F. Adler, G. J. Huffman, X. Jin, S. Kato, N. G. Loeb, P. W. Stackhouse, R. A. Weller, and A. C. Wilber

The ocean and atmosphere communicate via interfacial exchanges of heat, freshwater, and momentum. These air–sea

fluxes are the primary mechanisms for keeping the global climate system in balance with the incoming insolation at Earth’s surface. Most of the shortwave radiation (SW) absorbed by the ocean’s surface is vented into the atmosphere by three processes: longwave radiation (LW), turbulent heat loss by evaporation (latent heat flux, or LH), and turbulent heat loss by conduction (sensible heat flux, or SH). The residual heat is stored in the ocean and transported away by the ocean’s surface circulation, forced primarily by the momentum transferred to the ocean by wind stress. Evaporation connects heat and moisture transfers, and the latter, together with pre-

cipitation, determines the local surface freshwater flux. Identifying changes in the air–sea fluxes is essential in deciphering observed changes in ocean circulation and its transport of heat and salt from the tropics to the poles. In particular, 2015 witnessed the interplay of three different warmings: the warm “Blob” in the

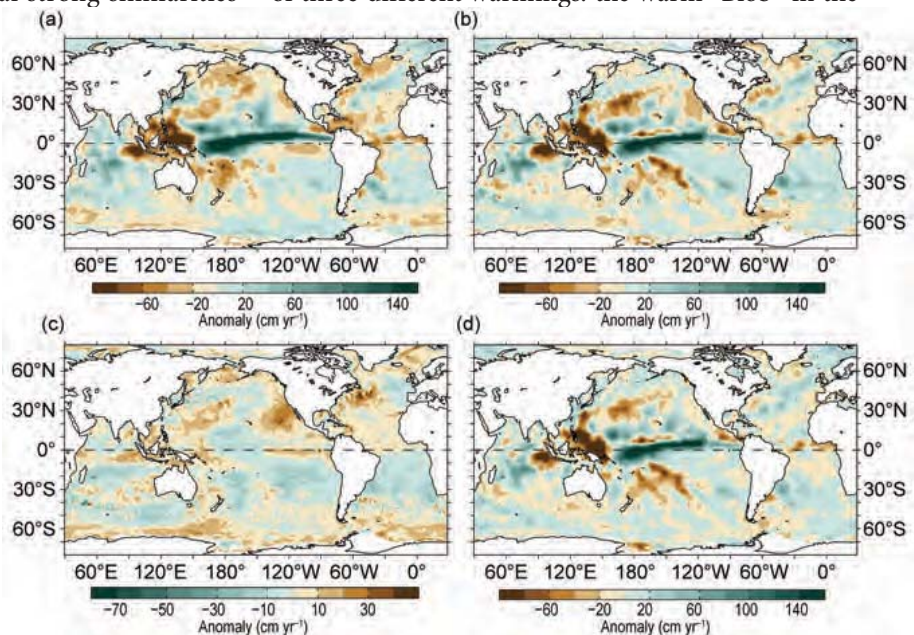


FIG. 3.12. (a) Surface freshwater ($P-E$) flux anomalies for 2015 relative to a 27-year (1988–2014) climatology. 2015–2014 anomaly tendencies for (b) $P-E$, (c) evaporation (E), and (d) precipitation (P), respectively. Green colors denote anomalous ocean moisture gain, and browns denote loss, consistent with the reversal of the color scheme in (c). P is computed from the GPCP version 2.2 product, and E from OAFIux high-resolution satellite-based analysis.